Brain-Heart-Gut Guided Multi-Constraint Knowledge Distillation for Early Alzheimer's Disease Diagnosis

Fan Li[1,2,3], Shilun Zhao[1], Shuwei Bai[1,5], Yuxiao Liu[1], Kai Zhang[1], Yin Xu[2], Ya Zhang[3,4], Kaicong Sun[1] (✉), Dinggang Shen[1,5,6] (✉)

[1] School of Biomedical Engineering & State Key Laboratory of Advanced Medical Materials and Devices, ShanghaiTech University, Shanghai 201210, China
[2] Cooperative Medianet Innovation Center, Shanghai Jiao Tong University, Shanghai, 200240, China
[3] Shanghai Artificial Intelligence Laboratory, Shanghai, 200232, China
[4] School of Artificial Intelligence, Shanghai Jiao Tong University, Shanghai, 200240, China
[5] Shanghai Clinical Research and Trial Center, Shanghai, 201210, China
[6] Shanghai United Imaging Intelligence Co., Ltd., Shanghai 200230, China
sunkc@shanghaitech.edu.cn, dgshen@shanghaitech.edu.cn

Abstract. Alzheimer's disease (AD) is a progressive and irreversible brain disorder. Emerging evidence suggests that Aβ deposition in the heart and microbiota dysbiosis in the gut may also contribute to the pathogenesis of AD. However, currently no studies have integrated heart and gut imaging information into AD diagnosis. To address this gap, we propose the first framework to integrate brain, heart, and gut information based on whole-body PET imaging and leverage these multi-organ interactions to guide brain-only model for early AD diagnosis in clinical applications. To this end, we collect multi-cohort data, including 1,475 unlabeled whole-body FDG-PET images, 1,730 brain FDG-PET images, and 70 labeled high-quality whole-body FDG-PET images. Our AD diagnostic model consists of two stages: (1) feature extraction and alignment, where AD-related features across brain, heart, and gut are extracted and aligned via hierarchical Transformers using contrastive learning; and (2) multi-constraint knowledge distillation, which utilizes sample-level contrastive distillation, group-level distribution distillation, and response-level distillation to transfer the performance of brain-heart-gut model to the brain-only model. Experimental results show that, guided by the learned interactions of brain, heart, and gut, our brain-only model improves the area under the receiver operating characteristic curve (AUC) from 75.4% to 80.3% for normal control *vs.* mild cognitive impairment (MCI) classification, achieving comparable diagnostic performance of using whole-body PET.

Keywords: Alzheimer's disease · Brain-heart-gut · Whole-body PET · Knowledge distillation.

F. Li and S. Zhao—These authors contributed equally to this work.

1 Introduction

Alzheimer's disease (AD) is a progressive and irreversible brain neurodegenerative disorder characterized by memory loss and cognitive impairment [10,3]. Over 50 million people worldwide are affected by AD or other forms of dementia, and the number will triple and reach more than 150 million by 2050 [14]. Therefore, early diagnosis and intervention of AD becomes increasingly important. Over the past few decades, numerous brain imaging-based methods have been developed for early AD diagnosis [2]. Nevertheless, AD is a multifactorial disease, and its progression is strongly influenced by peripheral organs [22]. The brain-centric perspective, which focuses solely on brain imaging, may overlook the impact of systemic factors and has nearly reached its performance upper bound within the current network architecture. Integrating insights from peripheral organs could further enhance the performance for early AD diagnosis.

Several hypotheses have been proposed to explain brain-organ interactions for AD, with a particular focus on brain-heart and brain-gut [17,20], respectively. A key hypothesis suggests that pathological molecular deposits in the heart and gut may contribute to brain damage, offering a potential pathway for early AD diagnosis [9,18,8]. However, the existing studies mostly rely on biofluid analyses, which have not leveraged multi-organ molecular imaging for early AD diagnosis.

In the last decade, deep learning has been widely applied to early AD diagnosis, evolving from CNN to Transformer and from single modality to multiple modalities [11,4,6,19,24,21,12]. Recent studies intend to exploit multi-modal data to improve the diagnosis performance. For instance, Sun et al. [19] proposed a synthesis-empowered uncertainty-aware classification network for AD diagnosis to achieve multi-modal classification using single-modal input via hierarchical constraint-based modality synthesis. Despite the use of multiple modalities, these methods are limited to the information of brain. To the best of our knowledge, there is no AI-assisted research targeting early AD diagnosis by integrating brain, heart, and gut data, leaving the interactions of these organs unexplored.

To address these issues, we aim to use whole-body 2-meter panoramic PET [1] and multi-organ alignment to characterize brain-organ metabolic connectivity and conduct whole-body studies of AD. Moreover, due to the scarcity of whole-body PET scanners in clinics, we further propose to transfer the learned brain-heart-gut correlations to the brain-only model by multi-constraint knowledge distillation to achieve comparable diagnostic performance of using whole-body PET. To be specific, our framework comprises three stages. In Stage I, our model is pretrained on 1,730 brain PET images and 1,475 unlabeled whole-body PET images based on self-supervised learning. In Stage II, the pretrained model is finetuned on 70 high-quality whole-body PET images with diagnosis labels, where hierarchical Transformers with contrastive learning (CL) are employed to align the heart and gut features towards brain to ease their integration for improved diagnosis. In Stage III, a multi-constraint knowledge distillation framework including sample-level contrastive distillation, group-level distribution distillation, response-level knowledge distillation is introduced to transfer the integrated brain-heart-gut features to the brain-only model. Therefore, the main contributions of this work

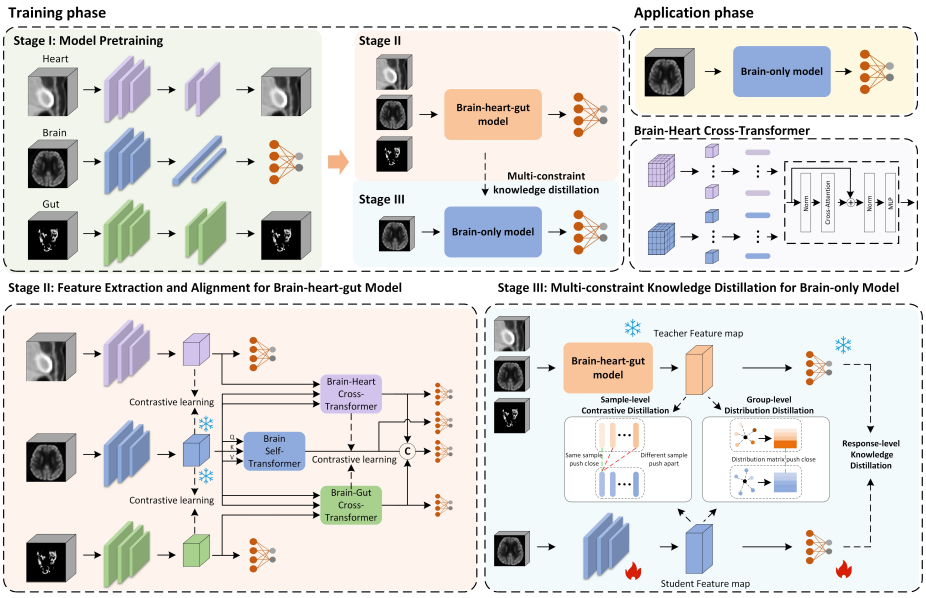

Fig. 1. Illustration of our proposed method. We use whole-body PET images in the training phase to guide the early AD diagnosis of using brain-only images during the inference phase.

include: 1) development of the first AD diagnosis framework by integrating brain, heart, and gut at the molecular level using whole-body PET imaging; 2) introduction of an advanced feature extraction and alignment scheme based on hierarchical Transformers and CL, effectively aligning and integrating brain, heart, and gut features; 3) design of a multi-constraint knowledge distillation mechanism by capturing holistic cross-sample correlations, aligning inter-category feature variations, and optimizing sentiment decision boundaries, to enhance the transfer of brain-heart-gut features to brain features.

2 Method

The overall framework is illustrated in Fig. 1. The training phase has three stages including 1) model pretraining; 2) feature extraction and alignment for brain-heart-gut model; 3) multi-constraint knowledge distillation for brain-only model. In the inference phase, only brain PET images are needed and can achieve comparable diagnosis performance as using whole-body PET images. More detailed descriptions are given in the following sections.

2.1 Model Pretraining

To fully use the collected unlabeled whole-body PET and labeled brain PET images, we pretrain the image encoders of brain, heart, and gut individually. To

pretrain the brain model, we develop a classification network based on ResNet-34 [5], utilizing brain PET images from ADNI [7,13,16] and Huashan (HS) Hospital. To pretrain the heart and gut models, we leverage heart and gut images from the whole-body PET data acquired at the Hangzhou Universal Medical (HZUM) Imaging Diagnostic Center. Since this dataset lacks disease-related labels, we employ self-supervised reconstruction to pretrain autoencoders for the heart and gut. The image encoders are also ResNet-34, and the image decoders consist of four convolutional layers. The datasets are split into 7:1:2 for training, validation, and test. To maximize the utility of our dataset, we further apply data augmentation for training set including intensity scaling ($0.95-1.05$), rotation (± 10 degrees), and translation (within 10% of the image dimensions).

2.2 Feature Extraction and Alignment for Brain-heart-gut Model

The primary goal of Stage II is to achieve improved diagnostic performance compared to the single-modal model through feature alignment and integration of brain, heart, and gut. We finetune the pretrained model on whole-body PET images by utilizing 1) contrastive learning (CL) to extract and align disease-related heart and gut features towards brain features; 2) hierarchical Transformer blocks to integrate brain-heart and brain-gut features.

Specifically, we employ the pretrained ResNet-34 encoders followed by several convolutional layers to extract feature maps (with identical dimension) of brain, heart, and gut. To extract disease-relevant and fusion-friendly features from the heart and gut, we apply CL to facilitate their alignment with brain features. Specifically, we freeze the brain features and impose similarity match between the brain-heart features and the brain features. We perform the same approach for the brain-gut features. In our experiments, given a mini-batch of B samples $\{m_0, m_1, \cdots, m_B\}$, the extracted feature maps F_{b}, F_{h}, and F_{g} all have the same size of $\mathrm{B} \times 512 \times 16 \times 16 \times 16$. These feature maps are averaged along the channel dimension and flattened to a size of $\mathrm{B} \times 4096$. To compute the CL between the brain and heart features, we transpose the brain features and multiply them with the heart features, resulting in a similarity matrix $\boldsymbol{P}^{\mathrm{b,h}}$ of size $\mathrm{B} \times \mathrm{B}$. Similarly, we can also obtain the similarity matrix $\boldsymbol{P}^{\mathrm{b,g}}$ for brain and gut. In the meanwhile, we can construct the ground-truth similarity matrices $\boldsymbol{y}^{\mathrm{b,h}}$ and $\boldsymbol{y}^{\mathrm{b,g}}$ for CL, where the values corresponding to the same subject or the same classification label are set to 1, and the remaining values are set to 0. It encourages the samples with the same label to be clustered and with different labels to be pushed apart.

Subsequently, these extracted and aligned features of different organs are fused through hierarchical Transformer blocks. To be specific, the feature maps F_{b}, F_{h}, and F_{g} are divided into $4 \times 4 \times 4$ patches with each patch added with positional encodings, resulting in the size of $\mathrm{B} \times 64 \times 64$. The brain features are first passed through a self-Transformer block to obtain features F_{bs}. Brain-heart features are fused through a cross-Transformer block, where brain features are projected as K and V, while heart features are projected to Q. The same strategy is applied to brain-gut and brain. After fusion, we obtain features F_{bh} and F_{bg}, and these

features are aligned for consensus using CL following the same procedure as before. The CL loss L_{CL} is formulated as:

$$L_{\mathrm{CL}} = -\frac{1}{B}\sum_{i=1}^{B}\sum_{j=1}^{B}\Big(y^{\mathrm{b,h}}_{m_i,m_j}\log(p^{\mathrm{b,h}}_{m_i,m_j}) + y^{\mathrm{b,g}}_{m_i,m_j}\log(p^{\mathrm{b,g}}_{m_i,m_j}) + y^{\mathrm{bh,bg}}_{m_i,m_j}\log(p^{\mathrm{bh,bg}}_{m_i,m_j}) + y^{\mathrm{bg,bh}}_{m_i,m_j}\log(p^{\mathrm{bg,bh}}_{m_i,m_j})\ \Big) \tag{1}$$

Finally, the fused features F_{bs}, F_{bh}, and F_{bg} are concatenated to form F_{bhg}. The feature maps F_{h}, F_{g}, F_{bs}, F_{bh}, F_{bg}, and F_{bhg}, are passed into the individual classifiers with cross-entropy as the classification loss. Therefore, the overall loss for Stage II can be formulated below:

$$L_{\mathrm{StageII}} = \lambda_1(L_{\mathrm{h}} + L_{\mathrm{g}}) + \lambda_2(L_{\mathrm{bs}} + L_{\mathrm{bh}} + L_{\mathrm{bg}}) + \lambda_3 L_{\mathrm{bhg}} + \lambda_4 L_{\mathrm{CL}} \tag{2}$$

where L_{h}, L_{g}, L_{bs}, L_{bh}, L_{bg} and L_{bhg} are the cross-entropy losses, with the weighting parameters tuned as $\lambda_1 = 1$, $\lambda_2 = 0.8$, $\lambda_3 = 1.2$, $\lambda_4 = 0.3$.

2.3 Multi-constraint Knowledge Distillation for Brain-only Model

In this stage, the objective is to enhance the diagnostic performance of the brain-only model under the guidance of brain-heart-gut features. To achieve this, we propose a multi-constraint knowledge distillation framework for knowledge transfer, comprising sample-level contrastive distillation (SCD), group-level distribution distillation (GDD), and response-level knowledge distillation (RKD). This mechanism endows the brain-only model to benefit from the trained brain-heart-gut network.

The proposed SCD enhances holistic knowledge encoding by applying CL to the sample-level representations. Specifically, brain-heart-gut representations and brain representations from the same sample are similar, while those from different samples remain distinct. We compute the similarity matrix $\boldsymbol{P}^{\mathrm{bhg,b}}$ by multiplying the network's representations, resulting in a matrix of size B × B, where B is the number of samples in a mini-batch. Additionally, we construct the contrastive loss matrix $y^{\mathrm{bhg,b}}_{m_i,m_j}$, where the diagonal values are 1 and the off-diagonal values are 0. The loss L_{SCD} can be can be formulated as:

$$L_{\mathrm{SCD}} = -\frac{1}{M}\sum_{m_i=1}^{M}\sum_{m_j=1}^{M} y^{\mathrm{bhg,b}}_{m_i,m_j}\log(p^{\mathrm{bhg,b}}_{m_i,m_j}) \tag{3}$$

Moreover, GDD is based on the core idea of refining and transferring knowledge regarding group feature variations to address the issue of ambiguous feature distributions. Formally, we denote the features of each sample as H^w_k, with $w \in \{\mathrm{bhg}, \mathrm{b}\}$, $k \in \{\mathrm{MCI}, \mathrm{NC}\}$. The group feature variation matrix is defined as follows:

$$M^w_k(i) = \frac{H^w_k(i)\,(G^w_k)^\top}{\|H^w_k(i)\|_2 \|G^w_k\|_2} \tag{4}$$

where $M_k^w(i)$ denotes the similarity between the sample i and the group representation G_k^w in network w. The brain-heart-gut and brain networks compute distribution matrices M_k^{bhg} and M_k^{b}, respectively. We minimize the squared Euclidean distance between these distribution matrices to maintain consistency. The loss L_{GDD} can be formulated as:

$$L_{\text{GDD}} = \frac{1}{B}\sum_{i=1}^{B}(\left\|M_{\text{MCI}}^{\text{bhg}}(i) - M_{\text{MCI}}^{\text{b}}(i)\right\|_2 + \left\|M_{\text{NC}}^{\text{bhg}}(i) - M_{\text{NC}}^{\text{b}}(i)\right\|_2) \tag{5}$$

The RKD employs the Kullback-Leibler (KL) similarity measure to maintain information consistency between the brain-heart-gut and brain networks. The loss L_{RKD} is defined as

$$L_{\text{RKD}} = t^2 \times KL(p^{\text{bhg}}||p^{\text{b}}), \tag{6}$$

where t means temperature, set to 2, and p^{bhg}, p^{b} denote the predict scores of brain-heart-gut and brain network, respectively.

The overall training objective L_{StageIII} is expressed as $L_{\text{StageIII}} = \lambda_5 L_{\text{cls}} + \lambda_6 L_{\text{SCD}} + \lambda_7 L_{\text{GDD}} + \lambda_8 L_{\text{RCD}}$,where L_{cls} is the cross-entropy loss, and λ_5, λ_6, λ_7, λ_8 are the weighting factors for the loss terms, set to 1, 0.3, 0.3, 0.3, respectively.

3 Experiments

3.1 Materials and Experimental Setup

Our framework was evaluated on a relatively large set of paired whole-body PET/CT and brain PET/MRI data from multiple cohorts. The study population and characteristics are summarized in Table 1. For whole-body PET/CT data, we utilized two datasets: the Hangzhou Universal Medical (HZUM) Imaging Diagnostic Center (n=1475 without AD diagnosis labels) and Zhongshan (ZS) Hospital (n=70 with AD diagnosis labels). For brain PET/MRI, we collected 1,242 PET/MRI scans from ADNI, 488 PET/MR scans from Huashan (HS) Hospital, and 49 PET/MR scans from Zhongshan (ZS) Hospital. All T1-weighted brain MRI scans underwent a standard pipeline for preprocessing, including intensity correction, skull-stripping, and linear alignment to the Montréal Neurological Institute (MNI) template. Each PET scan was aligned with its corresponding MR image and transformed to the MNI template using the affine matrix derived from the corresponding MR image. For heart and gut images, we resampled them to the same isotropic spacing of $1 \times 1 \times 1\ mm^3$ as the brain images.

In our implementation, models were optimized using SGD optimizer. The initial learning rate was set as 10^{-3}, and the mini-batch size was set as 8. We trained the models using PyTorch on a single NVIDIA A100 GPU equipped with 80GB RAM. Across all the experiments, our models were evaluated by AUC, accuracy (ACC), sensitivity (SEN), specificity (SPE), and F1-score (F1) with mean value and standard deviation of five-fold cross-validation. The source code is publicly available at https://github.com/lifan0321/BHG-distillation.

Table 1. Study population and characteristics.

Dataset	Modality	Age	Gender(M/F)	Education	MMSE
ZS Hospital					
NC [n=43]	whole-body PET/CT	65.7 ± 7.0	19/24	12.4 ± 3.2	-
MCI [n=27]	whole-body PET/CT	68.1 ± 9.6	10/17	10.4 ± 2.2	-
NC [n=27]	brain PET/MRI	60.8 ± 8.8	10/17	10.2 ± 4.1	-
MCI [n=22]	brain PET/MRI	69.6 ± 9.2	6/16	11.2 ± 2.9	-
HZUM Imaging Diagnostic Center					
None [n=1475]	whole-body PET/CT	59.7 ± 14.2	807/668	-	-
ADNI					
NC [n=400]	brain PET/MRI	73.6 ± 5.9	196/204	16.4 ± 2.7	28.9 ± 1.2
MCI [n=842]	brain PET/MRI	72.8 ± 7.5	486/356	16.1 ± 2.7	27.8 ± 1.8
HS Hospital					
NC [n=345]	brain PET/MRI	63.9 ± 7.7	119/216	12.3 ± 3.1	28.0 ± 1.6
MCI [n=143]	brain PET/MRI	65.6 ± 6.8	57/86	11.2 ± 3.0	26.2 ± 1.9

Table 2. Performance for NC *vs.* MCI classification based on ZS data.

Method	ACC	SEN	SPE	F1	AUC
B	0.665 ± 0.098	0.603 ± 0.097	0.708 ± 0.146	0.586 ± 0.088	0.754 ± 0.051
BH	0.714 ± 0.041	0.653 ± 0.237	0.751 ± 0.119	0.616 ± 0.109	0.797 ± 0.062
BG	0.709 ± 0.121	0.647 ± 0.230	0.765 ± 0.217	0.625 ± 0.150	0.794 ± 0.101
BHG	0.744 ± 0.088	0.680 ± 0.217	0.793 ± 0.075	0.659 ± 0.134	0.816 ± 0.071
BH guided	0.703 ± 0.048	0.630 ± 0.159	0.753 ± 0.136	0.613 ± 0.049	0.789 ± 0.063
BG guided	0.690 ± 0.064	0.620 ± 0.193	0.744 ± 0.085	0.597 ± 0.085	0.784 ± 0.092
Ours	$\mathbf{0.730 \pm 0.063}$	$\mathbf{0.657 \pm 0.236}$	$\mathbf{0.773 \pm 0.141}$	$\mathbf{0.626 \pm 0.152}$	$\mathbf{0.803 \pm 0.084}$

3.2 Performance of Proposed Method

To evaluate the effectiveness of our proposed framework, we explore its performance under different input combinations and summarize the results in Table 2. The 1st to 4th rows in the table show the results of Stage II, which demonstrates the impact of heart and gut on early AD diagnosis. It turns out that incorporating heart and gut information enhances diagnostic performance. The 5th to 7th rows analyze the guidance from different interactions for brain-only early AD diagnosis. The results indicate that guidance from other organs can indeed improve the brain-only model, and our model (guided by brain, heart, and gut) achieves comparable performance as using whole-body PET (4th row).

3.3 Ablation Study

We conducted an ablation study to evaluate the impact of the key components in our framework, with results presented in Table 3. First, removing CL in Stage II leads to a performance decline because CL aligns heart and gut features with brain features, making them more disease-relevant and fusion-friendly. Second, in Stage III, progressively removing each knowledge distillation constraint reduces the model's performance, indicating that both CL and multi-constraint knowledge distillation are crucial in our framework.

Table 3. Ablation study for NC *vs.* MCI classification based on ZS data.

Method	ACC	SEN	SPE	F1	AUC
Ours (w/o CL)	0.704 ± 0.081	0.603 ± 0.232	0.766 ± 0.101	0.586 ± 0.177	0.776 ± 0.085
Ours (w/o SCD)	0.691 ± 0.077	0.590 ± 0.223	0.753 ± 0.135	0.570 ± 0.154	0.780 ± 0.086
Ours (w/o GDD)	0.705 ± 0.074	0.627 ± 0.239	0.752 ± 0.251	0.609 ± 0.072	0.789 ± 0.105
Ours (w/o RKD)	0.717 ± 0.070	0.620 ± 0.220	0.768 ± 0.104	0.611 ± 0.130	0.794 ± 0.065
Ours	$\mathbf{0.730 \pm 0.063}$	$\mathbf{0.657 \pm 0.236}$	$\mathbf{0.773 \pm 0.141}$	$\mathbf{0.626 \pm 0.152}$	$\mathbf{0.803 \pm 0.084}$

Table 4. Performance of representative methods for NC *vs.* MCI classification based on ZS data.

Method	ACC	SEN	SPE	F1	AUC
ResNet-34	0.666 ± 0.075	0.636 ± 0.214	0.673 ± 0.121	0.575 ± 0.144	0.750 ± 0.057
SNet	0.662 ± 0.096	0.543 ± 0.185	0.723 ± 0.162	0.541 ± 0.117	0.740 ± 0.063
MiSePyNet	0.650 ± 0.097	0.580 ± 0.214	0.692 ± 0.265	0.554 ± 0.046	0.769 ± 0.059
Ours	$\mathbf{0.730 \pm 0.063}$	$\mathbf{0.657 \pm 0.236}$	$\mathbf{0.773 \pm 0.141}$	$\mathbf{0.626 \pm 0.152}$	$\mathbf{0.803 \pm 0.084}$

3.4 Comparison with Representative Brain-only Methods

To further evaluate our proposed method, we conducted quantitative comparison with several existing representative AD diagnosis methods, including ResNet-34 [5], SNet [23] and MiSePyNet [15]. For a fair comparison, all these methods were developed using the same dataset, the same data splitting scheme, and the same pretraining and finetuning stages. Quantitative results are provided in Table 4. Our method achieves the best performance, with the improvement primarily attributed to the additional guidance from the heart and gut. By capturing a broader spectrum of disease-related information, our model offers a more holistic perspective, leading to more accurate diagnostic outcomes.

3.5 Generalizability Study

To evaluate the generalizability of our framework, we applied few-shot learning to the public ADNI dataset and the in-house HS Hospital and ZS Hospital. Specifically, we selected 15, 10, and 5 samples per label from ADNI, HS Hospital, and ZS Hospital, respectively. We assessed two variants: 1) finetuning the weights of pretrained brain-only (B) model; 2) finetuning the weights of the pretrained BHG-guided B model, and summarize the results in Fig. 2. Our findings demonstrate that finetuning on BHG-guided model achieves the best performance across all the datasets, highlighting the robust generalizability of our framework.

4 Conclusions

In this paper, we propose the first framework that effectively integrates brain, heart, and gut information from whole-body PET images to guide brain-only early AD diagnosis. Leveraging the proposed multi-organ alignment and fusion, along with the multi-constraint knowledge distillation strategies, our BHG-guided

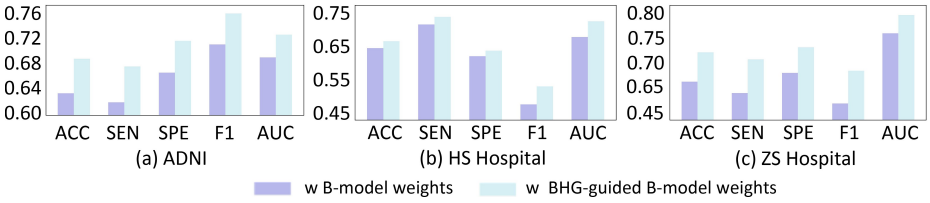

Fig. 2. Generalizability study on three datasets.

brain-only model can achieve comparable diagnosis performance as using whole-body PET images, which pushes the performance limit of early AD diagnosis further by resorting to the learned interactions among brain, heart, and gut.

Acknowledgments. This work was supported in part by National Natural Science Foundation of China (grant numbers U23A20295, 62131015, 62250710165, 82394432), the STI 2030-Major Projects (No. 2022ZD0209000), Shanghai Municipal Central Guided Local Science and Technology Development Fund (grant number YDZX20233100001001), The Key R&D Program of Guangdong Province, China (grant number 2023B0303040001) and HPC Platform of ShanghaiTech University.

Disclosure of Interests. The authors have no competing interests to declare that are relevant to the content of this article.

References

1. Alavi, A., Saboury, B., Nardo, L., Zhang, V., Wang, M., Li, H., Raynor, W.Y., Werner, T.J., Høilund-Carlsen, P.F., Revheim, M.E.: Potential and most relevant applications of total body pet/ct imaging. Clinical nuclear medicine **47**(1), 43–55 (2022)
2. Aramadaka, S., Mannam, R., Narayanan, R.S., Bansal, A., Yanamaladoddi, V.R., Sarvepalli, S.S., Vemula, S.L.: Neuroimaging in alzheimer's disease for early diagnosis: a comprehensive review. Cureus **15**(5) (2023)
3. BETTER, M.A.: Alzheimer's disease facts and figures. Alzheimer's Dement **20**, 3708–3821 (2024)
4. Fan, J., Cao, X., Wang, Q., Yap, P.T., Shen, D.: Adversarial learning for mono-or multi-modal registration. Medical image analysis **58**, 101545 (2019)
5. He, K., Zhang, X., Ren, S., Sun, J.: Deep residual learning for image recognition. In: Proceedings of the IEEE conference on computer vision and pattern recognition. pp. 770–778 (2016)
6. He, K., Gan, C., Li, Z., Rekik, I., Yin, Z., Ji, W., Gao, Y., Wang, Q., Zhang, J., Shen, D.: Transformers in medical image analysis. Intelligent Medicine **3**(1), 59–78 (2023)
7. Jack Jr, C.R., Bernstein, M.A., Fox, N.C., Thompson, P., Alexander, G., Harvey, D., Borowski, B., Britson, P.J., L. Whitwell, J., Ward, C., et al.: The alzheimer's

disease neuroimaging initiative (adni): Mri methods. Journal of Magnetic Resonance Imaging: An Official Journal of the International Society for Magnetic Resonance in Medicine **27**(4), 685–691 (2008)
8. Jin, J., Xu, Z., Zhang, L., Zhang, C., Zhao, X., Mao, Y., Zhang, H., Liang, X., Wu, J., Yang, Y., et al.: Gut-derived β-amyloid: Likely a centerpiece of the gut–brain axis contributing to alzheimer's pathogenesis. Gut Microbes **15**(1), 2167172 (2023)
9. Kleniuk, J., Edison, P.: Association of cardiovascular risk and sex with cortical tau deposition in cognitively normal and at-risk alzheimer's subjects: Neuroimaging/new imaging methods. Alzheimer's & Dementia **16**, e046050 (2020)
10. Knopman, D.S., Amieva, H., Petersen, R.C., Chételat, G., Holtzman, D.M., Hyman, B.T., Nixon, R.A., Jones, D.T.: Alzheimer disease. Nature reviews Disease primers **7**(1), 33 (2021)
11. Liu, M., Li, F., Yan, H., Wang, K., Ma, Y., Shen, L., Xu, M., Initiative, A.D.N., et al.: A multi-model deep convolutional neural network for automatic hippocampus segmentation and classification in alzheimer's disease. Neuroimage **208**, 116459 (2020)
12. Liu, M., Zhang, D., Adeli, E., Shen, D.: Inherent structure-based multiview learning with multitemplate feature representation for alzheimer's disease diagnosis. IEEE Transactions on Biomedical Engineering **63**(7), 1473–1482 (2015)
13. Mueller, S.G., Weiner, M.W., Thal, L.J., Petersen, R.C., Jack, C.R., Jagust, W., Trojanowski, J.Q., Toga, A.W., Beckett, L.: Ways toward an early diagnosis in alzheimer's disease: the alzheimer's disease neuroimaging initiative (adni). Alzheimer's & Dementia **1**(1), 55–66 (2005)
14. Nichols, E., Steinmetz, J.D., Vollset, S.E., Fukutaki, K., Chalek, J., Abd-Allah, F., Abdoli, A., Abualhasan, A., Abu-Gharbieh, E., Akram, T.T., et al.: Estimation of the global prevalence of dementia in 2019 and forecasted prevalence in 2050: an analysis for the global burden of disease study 2019. The Lancet Public Health **7**(2), e105–e125 (2022)
15. Pan, X., Phan, T.L., Adel, M., Fossati, C., Gaidon, T., Wojak, J., Guedj, E.: Multi-view separable pyramid network for ad prediction at mci stage by 18 f-fdg brain pet imaging. IEEE Transactions on Medical Imaging **40**(1), 81–92 (2020)
16. Petersen, R.C., Aisen, P.S., Beckett, L.A., Donohue, M.C., Gamst, A.C., Harvey, D.J., Jack Jr, C., Jagust, W.J., Shaw, L.M., Toga, A.W., et al.: Alzheimer's disease neuroimaging initiative (adni) clinical characterization. Neurology **74**(3), 201–209 (2010)
17. Song, R., Pan, K.Y., Xu, H., Qi, X., Buchman, A.S., Bennett, D.A., Xu, W.: Association of cardiovascular risk burden with risk of dementia and brain pathologies: a population-based cohort study. Alzheimer's & Dementia **17**(12), 1914–1922 (2021)
18. Stakos, D.A., Stamatelopoulos, K., Bampatsias, D., Sachse, M., Zormpas, E., Vlachogiannis, N.I., Tual-Chalot, S., Stellos, K.: The alzheimer's disease amyloid-beta hypothesis in cardiovascular aging and disease: Jacc focus seminar. Journal of the American College of Cardiology **75**(8), 952–967 (2020)
19. Sun, K., Zhang, Y., Liu, J., Yu, L., Zhou, Y., Xie, F., Guo, Q., Zhang, H., Wang, Q., Shen, D.: Achieving multi-modal brain disease diagnosis performance using only single-modal images through generative ai. Communications Engineering **3**(1), 96 (2024)
20. Xiang, J., Tang, J., Kang, F., Ye, J., Cui, Y., Zhang, Z., Wang, J., Wu, S., Ye, K.: Gut-induced alpha-synuclein and tau propagation initiate parkinson's and alzheimer's disease co-pathology and behavior impairments. Neuron (2024)

21. Xue, C., Kowshik, S.S., Lteif, D., Puducheri, S., Jasodanand, V.H., Zhou, O.T., Walia, A.S., Guney, O.B., Zhang, J.D., Pham, S.T., et al.: Ai-based differential diagnosis of dementia etiologies on multimodal data. Nature Medicine **30**(10), 2977–2989 (2024)
22. Zhang, J., Zhang, Y., Wang, J., Xia, Y., Zhang, J., Chen, L.: Recent advances in alzheimer's disease: Mechanisms, clinical trials and new drug development strategies. Signal transduction and targeted therapy **9**(1), 211 (2024)
23. Zhang, Y., Sun, K., Liu, Y., Shen, D.: Transformer-based multimodal fusion for early diagnosis of alzheimer's disease using structural mri and pet. In: 2023 IEEE 20th International Symposium on Biomedical Imaging (ISBI). pp. 1–5. IEEE (2023)
24. Zhang, Y., Sun, K., Liu, Y., Xie, F., Guo, Q., Shen, D.: A modality-flexible framework for alzheimer's disease diagnosis following clinical routine. IEEE Journal of Biomedical and Health Informatics (2024)